Aircraft Observations of Turbulent Characteristics in the Tropical Cyclone Boundary Layer

Zhongkuo Zhao [1], P. W. Chan [2], Naigeng Wu[1], Jun A Zhang[3], K. K. Hon[2]

Received: 08 Jan 2019/ Accepted: DD Month YEAR/ Published online: DD Month YEAR

Abstract The Hong Kong Observatory conducted six flights in the atmospheric boundary layer of five Tropical cyclones off the coast of South China (Tropical Storm Jebi (1309), Typhoon Kalmaegi (1415), Severe Tropical Storm Linfa (1510), Typhoon Mujigae (1522) and strong Typhoon Nida (1604)). Three-dimensional wind data with 20 Hz sampling rate were collected at a height range of 500 to 670 m. The mean wind speed from these low-level flights ranged from about 10 to 62 m s^{-1}. Turbulent momentum flux and turbulence kinetic energy (e) were calculated directly using the eddy correlation method. Horizontal scales of turbulent eddies, vertical eddy diffusivity (K), and vertical turbulent mixing length scale were estimated indirectly. The dependence of the momentum flux, e, K, and vertical mixing length on wind speed and height were presented and compared with previous studies. It is found that K nearly logarithmically increases with the wind speed up to 40 m s^{-1} before leveling off, while the vertical mixing length is nearly constant and is ~100 m. The results of this study may serve as a significant reference for further parameterization of the tropical cyclone boundary layer.

Keywords Atmospheric turbulence direct measurement at 20 Hz · Ekman layer turbulent characteristic in typhoon · Typhoon over South China coast · Vertical eddy diffusivity estimations in high wind

✉ Zhongkuo Zhao
✉ email.zhaozk@gd121.cn

[1] Guangzhou Institute of Tropical and Marine Meteorology, China Meteorological Administration, Guangdong Province, 510645, China

[2] Hong Kong Observatory, Hong Kong, 000000, China

[3] NOAA/AOML/Hurricane Research Division & University of Miami/CIMAS, Florida, 33149, USA

1 Introduction

Dynamic processes in the atmospheric boundary layer play an important role in changes of tropical cyclone (TC) intensity (Charney and Eliassen 1964, Ooyama 1969), which is also one of the key focal points of current research (Fang et al. 2009, Foster 2009, Coronel et al. 2016, Kilroy et al. 2017, Ming and Zhang 2018, Tang et al. 2018, Zhang et al. 2018). Initially, it was believed that the role of boundary layer friction in TC intensification is that radial inflow caused by friction provides water vapor for the maintenance of deep convection in the TC core. Gradually, the accelerated rotation of the boundary layer eddy caused by the convergence of absolute angular momentum brought by radial inflow was also considered as a cause of TC intensification (Shapiro and Willoughby 1982, Pendergrass and Willoughby 2009). A large number of numerical simulation studies (Wong and Chan 2006, Gopalakrishnan et al. 2013, Zhu et al. 2014, Liu et al. 2017, Zhang and Pu 2017, Zhang et al. 2017a, Zhang et al. 2017b, Rai and Pattnaik 2018) show that the boundary layer processes can have a significant impact on many aspects, such as TC structure, path and intensity.

However, due to the limitations of observation techniques and other factors, we have little knowledge on the observation of turbulent processes in the TC boundary layer, especially the Ekman-like outer planetary boundary layer (Kepert 2012). Based on aircraft observations in three hurricanes, Zhang et al. (2011a) found that turbulent eddies within the horizontal scale between 500 and 3000 m contributed to most of the total momentum flux, and the vertical eddy diffusivity for momentum has a trend of logarithmical increase with the mean wind speed. Zhang and Drennan (2012) also studied vertical eddy diffusivity and corresponding variation with height based on observation results obtained from the Coupled Boundary Layer Air-sea Transfer (CBLAST(Black et al. 2007)) hurricane experiment. The results showed that for surface wind speed within a range of 18 to 30 m s^{-1}, the vertical eddy diffusivity of momentum is close to that of latent heat flux, while the vertical eddy diffusivity of sensible heat is much smaller. The vertical distributions of the above three

diffusivities are generally similar, increasing with height from the surface to the maximum in the thermal mixing layer and then decreasing with height. Their observations also showed that the momentum and latent heat are transported downgradient normally, while upgradient transfer of sensible heat may exist. Recently, Tang et al. (2018) estimated the vertical eddy diffusion coefficient and mixing length up to an altitude of 83 m based on observations obtained from a coastal wind tower during three landing typhoons in 2010. Their results showed that for wind speed up to about 30 m/s the vertical eddy diffusivity for wind with seaward fetch is significantly smaller than that for wind with landward fetch. However, due to safety constraints, only the United States has conducted direct observations of a small number of hurricane cores worldwide. Limited by various factors, other countries have little in the way of aircraft turbulence observation data pertaining to the typhoon boundary layer.

The Hong Kong Government Flying Service's Jetstream 4100 fixed wing aircraft was equipped with a meteorological measurement system by the Hong Kong Observatory in 2009 to carry out direct observations of the typhoon boundary layer off the coast of South China. According to the aircraft's observations of wind speed near Typhoon Molave's eye in 2009, Chan et al. (2011) supplied for the first time the estimation of a tropical cyclone intensity over the northern part of the South China Sea based on direct measurements.They also performed a spectral analysis for horizontal wind speed and estimated the turbulence kinetic energy and its dissipation rates. Chan et al. (2014) estimated the centre position and maximum wind speed of the typhoon based on the aircraft observation in strong Typhoon Utor (2013), and determined the gale-force wind radius and calculated the turbulence intensity of the typhoon. Since then, the Hong Kong Observatory has also carried out aircraft-based atmospheric boundary layer observations for several typhoons off the coast of South China including a number of eye penetrations, providing valuable data for the study of typhoon boundary layers off the coast of South China.

The observation of vertical mixing process in the typhoon boundary layer is currently one of the frontiers in the field of TC research. It is apparent that more observational facts are required to discover the boundary-layer turbulent mixing processes in tropical cyclones over the South China sea. However, due to the absence of observation, China still has not conducted such research. This study analyzed the vertical mixing characteristics of several landing typhoons' boundary layers using the atmospheric boundary layer reconnaissance flights of Hong Kong Observatory. The following contents are arranged as follows: in the second section the data and processing methods used are introduced while the third section includes a result analysis and comparison, and the fourth section includes a corresponding discussion and conclusion.

2 Observation Data and Analysis Method

The turbulence data used in this report were obtained from reconnaissance flight missions operated jointly by the Hong Kong Observatory and the Hong Kong Government Flying Service using a Jetstream 4100(J41), which was equipped with a 20Hz Integrated Meteorological Measurement System (AIMMS-20). For an overview of the AIMMS-20 system, please refer to (Beswick et al. 2008). Foster and Chan (2012) have discussed in detail post-processing of original data using the AIMMS-20 measurement system in order to improve the quality of data. They stated that the measurement accuracy of a typical AIMMS-20 flight after post-processing can be improved by 20 to 30 %. The data used were taken from observations obtained over nine flights, including Typhoon Molave in 2009, Tropical Storm(TS) Jebi in 2013, Typhoon Kalmaegi in 2014, Typhoon Mujigae and severe TS Linfa in 2015 and strong typhoon Nida in 2016, of which Typhoon Molave was subject to observation over three flights, Kalmaegi was subject to observation over two flights, and all other TCs were observed over one flight each. Inspection found that there were false oscillations in the wind speed component data of the second flight through Molave during the level flight period, which had a strong correlation with flight height and should be eliminated. In order to limit our analysis and research within the boundary layer of typhoon, we only

selected time periods when the level flight height was below 1000 m, and we preliminarily determined that data for a total of 6 flights were left after the inspection and observation height limit. Subsequently, we mainly used three methods for data quality control: a turbulence spectrum -5/3 regular check, turbulence stationarity check and cumulative spectrum stabilization check. Similar method was used by French et al. (2007), Drennan et al. (2007) and Zhang et al(2008; 2009; 2011) for quality control and leg selection for flux calculation.

In order to determine whether the aircraft sampling covered all motion scales, the power spectral density of each wind speed component was calculated bythe Lomb-Scargle algorithm(Trauth 2015), due to that some of the time series were not evenly sampled. A power spectrum was close to a -5/3 power law in a wide frequency band (inertial sub-region). As shown in Fig.1, there was a subrange in each panel where the slope of the 20Hz wind speed and power spectrum of temperature detected by the aircraft in the double logarithmic coordinate system was very close to the ideal -5/3, which is known as the inertial subrange. However, data from some time periods deviated from the -5/3 slope, and we paid special attention to the data characteristics of these time periods in our analysis accordingly. If the corresponding physical parameters deviated significantly from the ensemble average, they were eliminated.

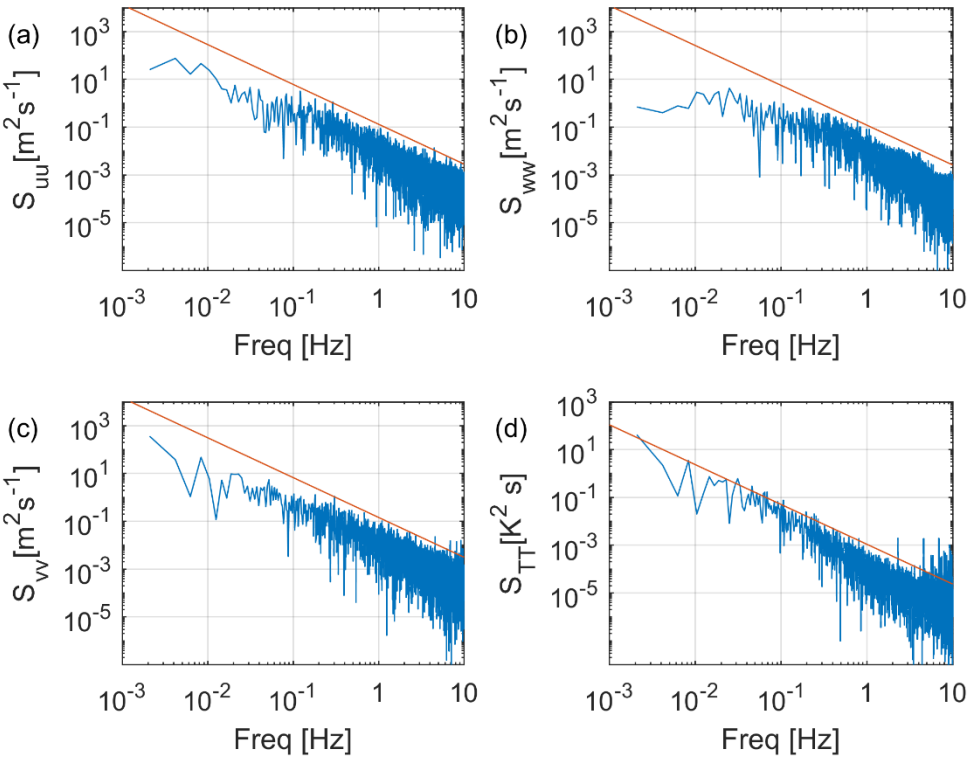

Fig.1 Power spectral density of Tropical Storm Jebi (2013) (2013-08-01 0147 UTC to 0156 UTC, 10 minutes total) derived from reconnaissance flight conducted by the Hong Kong Observatory; the straight red line is an ideal power function with an index of -5/3; (a) along wind, (b) vertical wind, (c) cross wind, and (d) temperature.

In the following data analysis, we found that vertical wind speed constitutes a key quantity, so we performed stationarity detection (Foken and Wichura 1996) for vertical wind speed as follows: first, we calculated the standard deviation σ of the 8-minute vertical wind speed data. Then, we divided the 8-minute data into 4 short segments of 2 minutes in length, and then calculated the 4 standard deviations in each intervaland their average σ_m . The stationarity test index *IST* is

$$IST = \left| \frac{\sigma - \sigma_m}{\sigma_m} \right|, \tag{1}$$

When $IST \leq 0.15$, the data quality is considered reliable.

The cumulative spectrum and cumulative co-spectrum, or cumulative frequency curve

(ogive) are commonly used in turbulence research to determine the appropriate length of time required to calculate turbulence flux (French et al. 2007). When estimating turbulent flux, a frequency accumulation curve can be used to understand the turbulent structure and spatial scale that contribute to turbulent transport. If the frequency accumulation curve tends toward a single value, it means that the averaging time length is suitable for calculating turbulence flux, and this limit value of the frequency accumulation curve represents the total variance and covariance or momentum flux. By checking, for example, Subfigures (b) and (d) shown later in Fig.5 and Fig.6, most of the frequency accumulation curves can be stabilized over an average time of eight minutes.

After the above-mentioned data screening and quality control, all observations of Typhoon Molave were excluded, and a total of 60 sections of data from six flights through the remaining five TCs were retained, i.e., a total time length of 480 minutes. The average observation heights of the 59 samples were concentrated within a height range of 500 to 670 m, and only the remaining one was a sample obtained at 945 m, as shown in Fig.2. Fig.3(a) shows the flight path corresponding to Fig.2 and the best path of the corresponding typhoon off the coast of South China, as well as the distance and orientation of the flight path relative to the centre of the corresponding typhoon (Fig.3b). It can be seen that most of the horizontal flight data were concentrated within a range of 400 km from the typhoon centre, and for Tropical Storm Jebi the right-front quadrant of 200 to 400 km from the typhoon centre was subject to measurement. For Mujigae and Linfa, the aircraft crossed the typhoon eye, while data collected for Typhoon Kalmaegi (one flight) and strong Typhoon Nida were also very close to the typhoon eye area, and the other flight in Typhoon Kalmaegi had a larger range of measurement, ranging from 266 to 600 km from the typhoon centre.

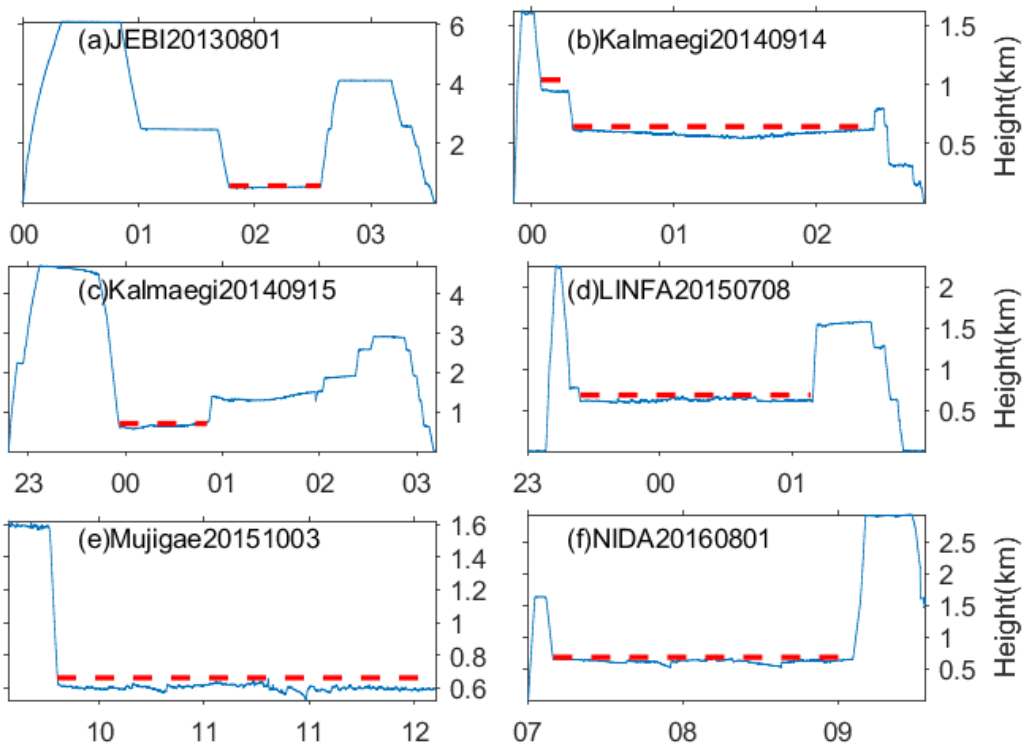

Fig.2 Flight altitude during the reconnaissance missions conducted by the Hong Kong Observatory for 5 TCs, including (a) tropical storm Jebi (1309), (b) and (c) typhoon Kalmaegi (1415), (d) severe tropical storm Linfa (1510), (e) typhoon Mujigae (1522) and (f) strong typhoon Nida (1604). The x-axes represent the UTC hour. The thick red dashed line corresponds to the level flying period used for analysis and calculation.

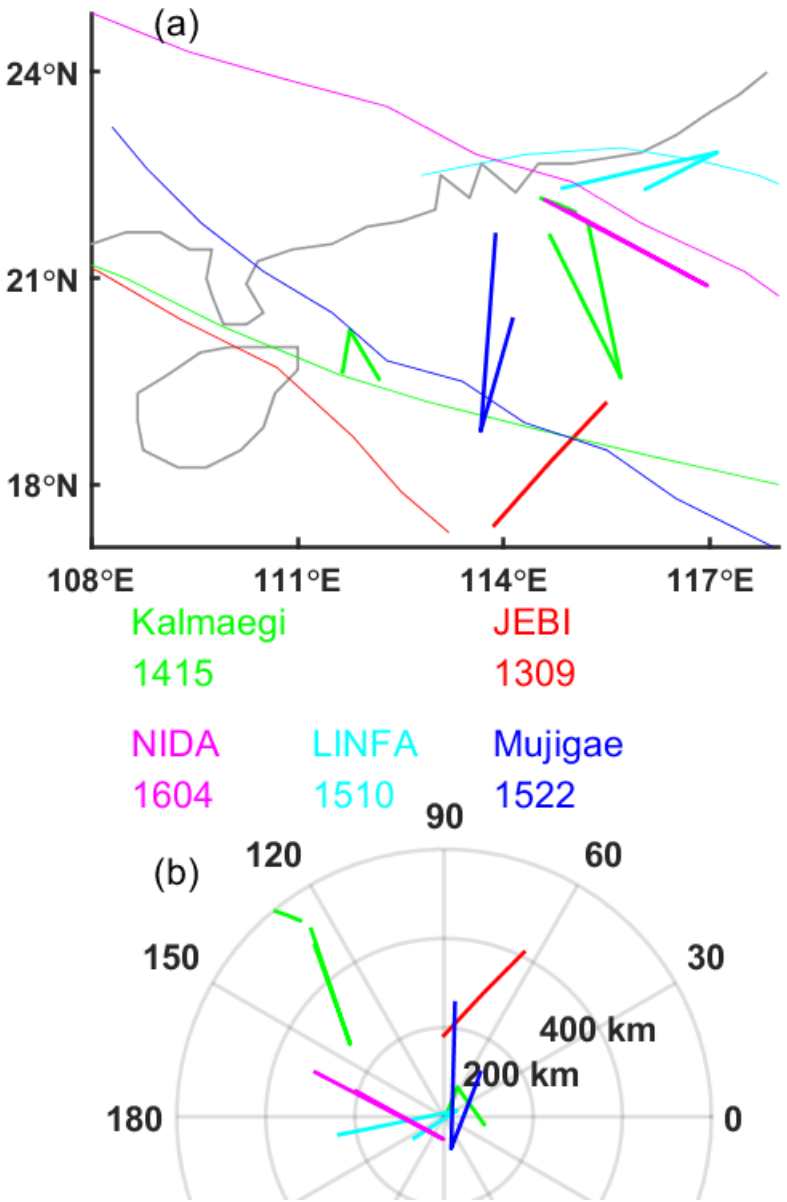

Fig.3 (a) The pathway of each tropical cyclone near south China and the aircraft during level flight over North of South China Sea; data showing the pathway of TCs were obtained from a data set of optimal pathways for typhoons provided by the China Meteorological Administration. The gray lines are the coastlines of South China Sea, and (b) the pathway of the aircraft during level flight in polar coordinates with respect to the corresponding typhoon centre is shown; the pathway of each typhoon is indicated by the same color as the aircraft observation pathway, with the aircraft observation track slightly thicker.

After quality enhancement and quality control was performed for aircraft turbulence data using the above post-processing technique, the momentum flux τ was calculated using the eddy-covariance technique.

$$\tau = \rho(-\overline{w'u'}\mathbf{i} - \overline{w'v'}\mathbf{j}), \quad (2)$$

where u, v and w represent the alongwind, crosswind and vertical wind speed components, respectively, the superscript represents perturbation values for each physical quantity, and ρ represents air density. The magnitude of τ is used in this paper. Turbulent perturbations are obtained by subtracting the linear least squares fit to the time series of wind components from the data after applying a high-pass filter with a cutoff frequency 0.001 Hz(Zhang et al. 2011a).

The calculation of turbulence kinetic energy (e) was based on the following formula:

$$e = 0.5(\overline{u'^2} + \overline{v'^2} + \overline{w'^2}). \quad (3)$$

According to the two parameterization schemes commonly used in the numerical model (Wang 2001), Hanna Method (Hanna 1968) and a method using turbulence kinetic energy(e) and dissipation rate (Holt and Raman 1988), we can estimate vertical eddy diffusivity. The two methods are briefly introduced here. Using the Hanna method (Hanna 1968), the eddy diffusivity K_1 can be estimated using the following formula:

$$K_1 = cl\sigma_w, \quad (4)$$

where the constant c=0.41following Nieuwstadt (1984), σ_w corresponds to the standard deviation of the vertical wind speed, l is the vertical mixing length

$$l = \sigma_w^3 / \varepsilon \quad (5)$$

and ε is the dissipation rate, which can be related with turbulence energy within the inertial subrange by

$$\varepsilon = \frac{2\pi}{U_{TAS}}\left[\overline{f^{5/3}S(f)} / \alpha\right]^{3/2}, \quad (6)$$

where f is the frequency, U_{TAS} is the true airspeed with respect to the aircraft, α is the Kolmogorov constant and set to a value of $\alpha = 0.5$ and $S(f)$ is the frequency-dependent power spectral density of the alond-wind speed. A mean value of ε is estimated over the frequency in the inertial subrange, where turbulence is assumed to be uniform and isotropic, and the power spectrum $S(f)$ conforms to a -5/3 power law. As shown by the two examples in Fig.5(a) and Fig.6(a), the power spectrum of the downwind component

can better match the form of a -5/3 power law in the frequency range of 0.4 to 4 Hz. By examining all the data, we found that most of the data do not deviate significantly from the - 5/3 power law within the 0.5 to 4 Hz range, so the above method is appropriate for estimating the turbulence dissipation rate.

Eddy diffusivity as estimated using e and dissipation rate (Holt and Raman 1988) corresponds to K_2

$$K_2 = c_2 e^2 / \varepsilon, \tag{7}$$

where the constant c_2 = 0.07 (Zhang and Drennan 2012).

In order to estimate the spatial scale of turbulent vortices, since the aircraft's airspeed is about 120 m s^{-1}, the time series measured by the aircraft can be converted into a spatial series and a power spectrum of the wavelength can be obtained according to Taylor's freezing hypothesis. Specifically, the average airspeed is divided by the frequency to obtain the wavelength, also referred to as the horizontal scale of the turbulent eddy.

3 Results

3.1 Spectral Analysis of Turbulent Eddy Structure

Based on the contribution of turbulent vortices at different scales to flux, co-spectra can be roughly classified into two categories: (1) Turbulent eddies at the horizontal scale of 1 to 10 km contribute continuously to momentum flux (variance) and play a dominant role in determining the sign of flux. There are 51 such samples, and Fig.5 (c)/(d) is one example; the corresponding crosswind component (in Fig. 4) shows sinelike variations, which are considered to be the signature of roll vortices(Zhu et al. 2010). (2) Turbulent vortices above a horizontal scale of 10 km contribute greatly to flux and determine the sign of flux. There are nine such samples remaining (2 for Jebi, 2 for Kalmaeji, 1 for Linfa, 2 for Mujigae and 2 for Nida), with the corresponding vertical eddy diffusivities that are generally high (as shown in next subsection) , and Fig.6 (c)/(d)

is one example during Typhoon Kalmaegi.The horizontal length scales were estimated from momentum cospectra and their ogive curves as upto which contributions to momentum flux are ⩾80% of the overall values. The horizontal length scales were estimated to range from 1 to 10 km mainly. The vertical mixing length obtained according to eq. (5) is taken as the vertical mixing scale, which is about 100 m on average. According to a rough estimation, the ratio of the horizontal scale to vertical scale for the turbulent eddy ranges from 10 to 100, fulfilling the geometric confinement for the existence of two-dimensional turbulence (Xia et al. 2009).

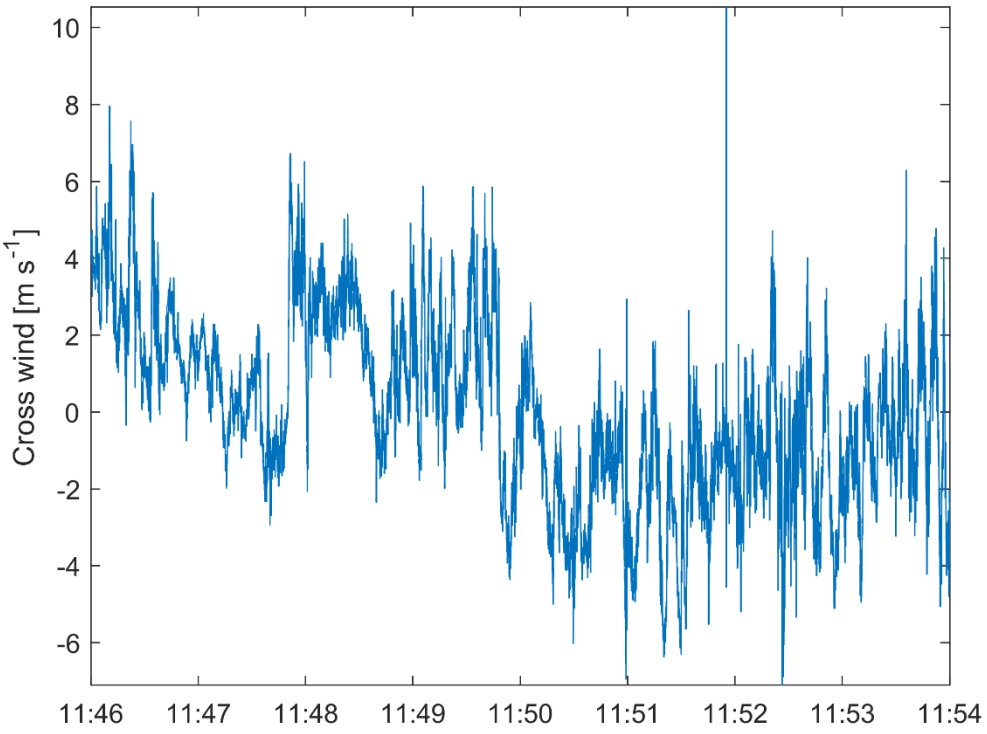

Fig. 4 Crosswind timeseries during 1146 to 1154 UTC on 03 Oct 2015

Here, we disscuss the possible structures corresponding to different scale eddies those have contributions to fluxes. These multi-km scale is within the width range of boundary layer rolls(Etling and Brown 1993, Morrison et al. 2005, Zhu et al. 2015). The crosswind components show sinusoidal fluctuations, as shown in Fig. 4, which were considered to be possibly associated with roll vortices(Zhu et al. 2010). An

analysis of Zhang et al. (2011a) shows that the horizontal scale of turbulent vortices contributing significantly to the flux of the eye wall boundary layer of hurricane Hugo was about 2 km, while hurricane Allen's situation is similar to hurricane Hugo, and the 500 to 3000 m turbulent eddy contributed most of the corresponding flux, which is significantly different from our analysis, which show a continuous contribution to flux from about 1km to 10 km. The contributions from scales 10 km and above are inferred to be related to the fine-scale spiral rainbands(Gall et al. 1998, Li et al. 2010), whose band width range from 5-15 km and band length vary from 10 to about 100 km. When the flight path is not perpendicular to the streamwise spiral bands, there will appear contributions to fluxes from scales above 10 km. Such finescale spiral rainbands are shown in Fig. 7., the flight were in regions with features of finescale spiral rainbands during the period of the data in Fig.6.

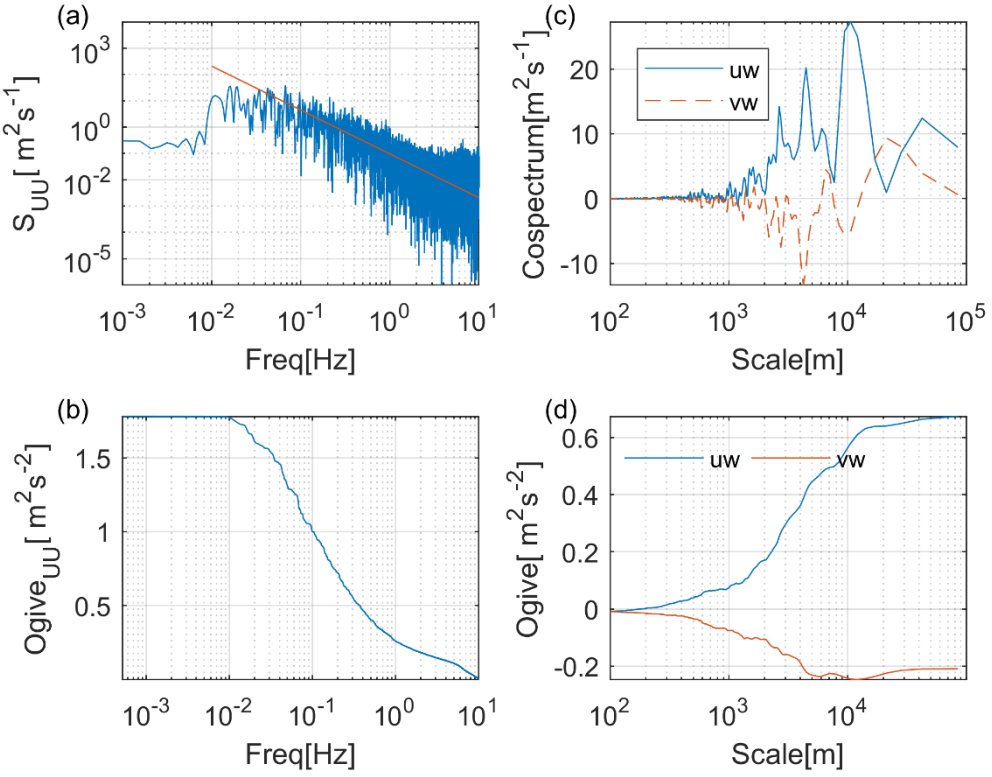

Fig.5 (a) alongwind wind speed spectrum, (b) alongwind wind speed spectrum Ogive, (c) co-spectrum of vertical wind speed *w* with alongwind *u* and crosswind *v*, respectively, (d) Ogive curve of two co-spectra. Data from Typhoon Mujigae (1522) 1146 to 1154 UTC of 3 October 2015

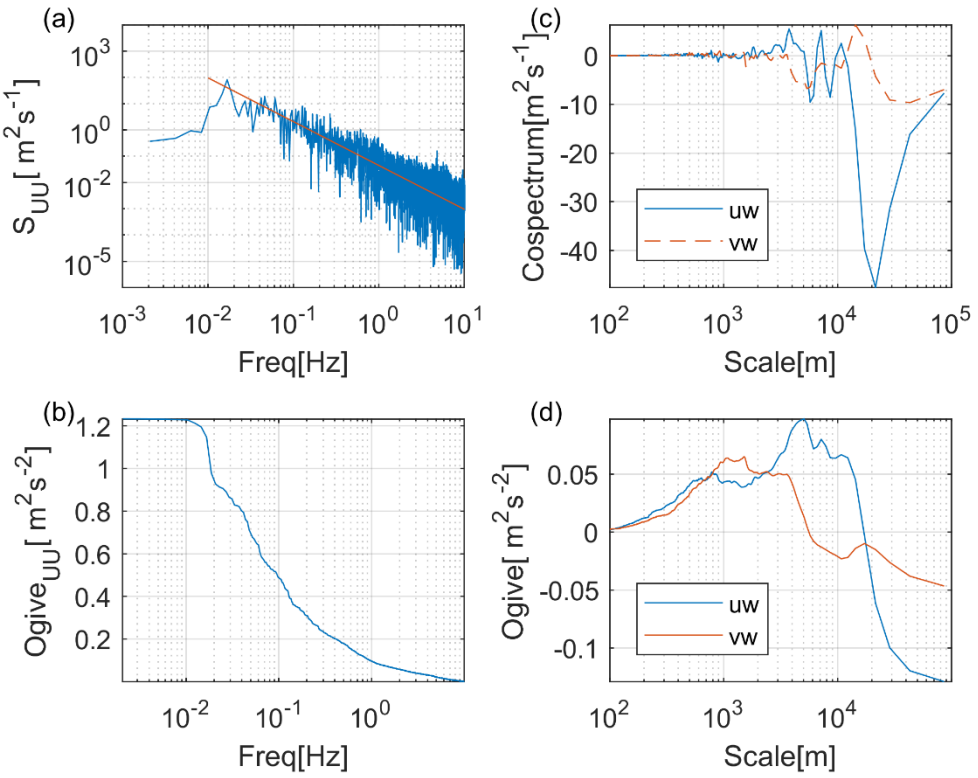

Fig.6 Same with Fig.4 but using data for Typhoon Kalmaegi (1415) obtained from 0137 to 0145 UTC2014-09-15

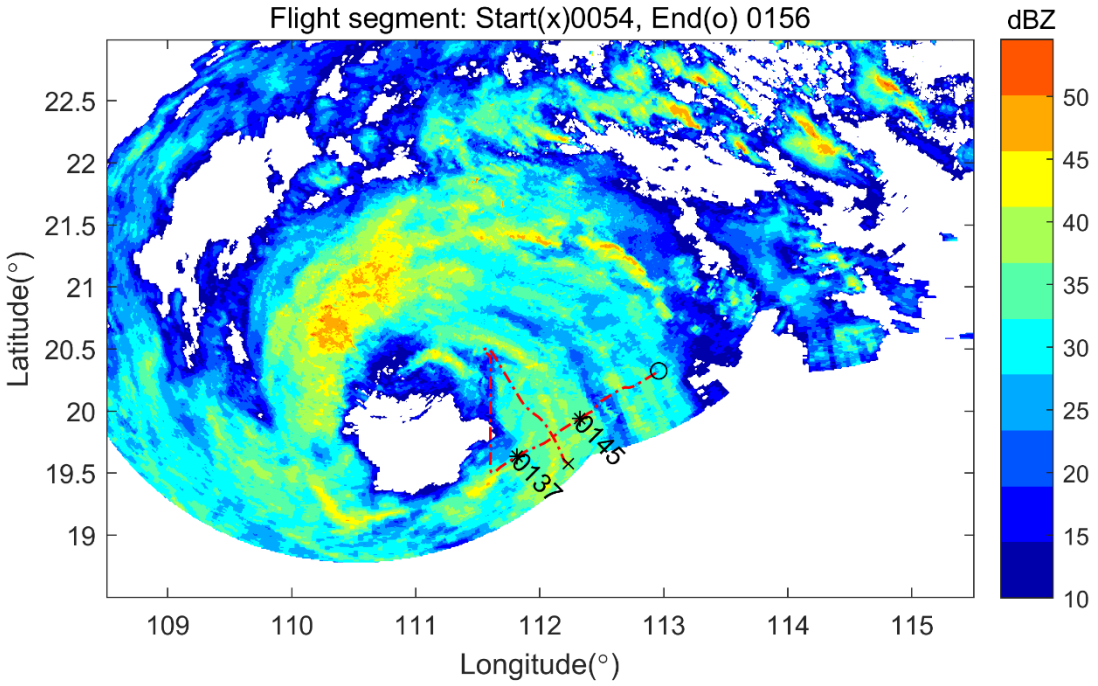

Fig. 7 The projection of the flight segment during Kalmaegi(1415) on the composite radar reflectivity at 3 km height at 0124 UTC 15 September 2014 from the South China weather radar network. The start and end of the flight segment are indicated by 'x' and 'o' mark, repectively. The 0137 and 0145 UTC 15 September 2014 are labelled with '*'.

3.2 Estimation of Turbulence Parameters

Specific values for τ and e are summarized in Table 1, and their changes with wind speed at the given flight altitude are shown in Fig.8. More than 90% of τ observation samples (55 out of 60 samples) were below 1.2 kg·m^{-1} s^{-2} and more than 80% of the samples (49 out of 60 samples) were below 0.8 kg·m^{-1} s^{-2}. Generally, when the wind speed is above 10 m s^{-1}, τ and e increase significantly with an increase in wind speed until the wind speed reaches a certain wind speed range (e.g., 35 to 40 m s^{-1}), and the local maximum of τ is about 0.8 kg·m^{-1} s^{-2} corresponding to a bin mean wind speed ≈ 37 m s^{-1}. Subsequently, the dependence of τ on wind speed weakens, and τ or e no longer increases significantly with wind speed but levels off, which is a similar

phenomenon with τ in high wind in the surface layer (Powell et al. 2003, Zhao et al. 2015). It should be noted that there are relatively few samples above 40 m s^{-1} and the dispersion among samples is large.

Differences are also shown between our results and those of Zhang et al. (2011a)in Fig.8(a). When the observation environment changes, the magnitude of τ changes also. Under the effects of the pressure gradient force and Coriolis force (Tennekes 1973), momentum flux will change with observation height, as can be seen in the momentum values of (Zhang et al. 2011a) at sea from 420 to 500 m; this is obviously higher than our result at the same wind speed, as shown in Fig.8(a) where the ratio between the two studies was about 2.2 for the bin-mean τ from 10 to 30 m s^{-1}. If the observation height decreases further, τ will increase continuously (French et al. 2007, Zhang and Drennan 2012), and when observations are performed in the surface layer, τ will reach its maximum (Powell et al. 2003, Zhao et al. 2015). The impact of surface roughness on momentum flux is more significant, and the momentum increase on land is more significant (Tang et al. 2018).

The turbulence kinetic energy (e) is generally not higher than 6 m^2 s^{-2}. The trend in e with the variation of wind speed at a given observation altitude is similar to that of τ. The values of 59 samples were below 8 m^2s^{-2}, and one sample with a value above 10 m^2s^{-2} was obtained from Nida in 2016 (start time: 0838 UTC 1 August 2016). According to the flight path in Fig. 10, this run of measurement was performed in a strongly echoic area of the typhoon eye wall. The observation results obtained by Zhang et al. (2011a) also include samples with a larger e. They believe that the e and momentum in the eyewall can reach 5-10 times that of outside the eyewall. The outlier sample in e above 10 m^2 s^{-2} of this paper was identified in the high reflectivity area of Nida's eye wall (as shown in Fig. 9), which is consistent with the previous studies (Zhang et al. 2011a). It can be noticed that there is an outlier of momentum flux (and eddy diffusivity in Fig.10) from strong Typhoon Nida in the lowest wind speed, which may be related to the substantial enhancement of air-sea drag effect as the wind decreases in low wind

regime(Zhu and Furst 2013). Zhu and Furst (2013) attibuted this phenomenon to the dependence of drag coefficient on turbulent intensity (*TKE*) in low wind regime. The corresponding *TKE* in the lowest wind speed does not follow the decreasing tendency in the higher wind regime, e.g., ~10 to ~35 m s^{-1}, although it is not obvious due to the large range of *TKE* in Fig.8(b). The data here confirms their statements.

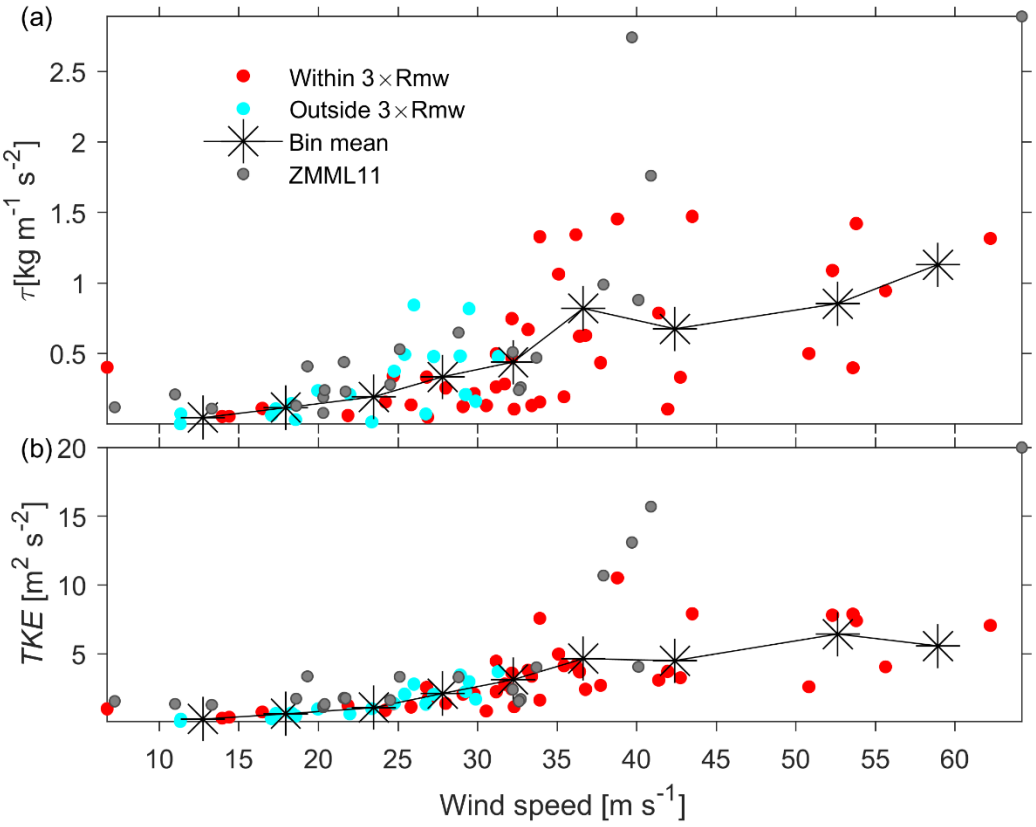

Fig.8 Changes in (a) momentum flux and (b) turbulence kinetic energy with the change in wind speed at the observed height in the five tropical cyclones. The samples are separated into 2 categories according to their distance to the typhoon center, one category of the samples is within the 3 times of radius of maximum wind, and the other category is outside the 3 times of radius of maximum wind. The curve shows the bin average value of the samples within the wind bin width of 5 m s^{-1}, and the two samples above 55 m s^{-1} fall into one interval. Some results of Zhang et al. (2011a)(ZMML11) are also quoted (not including the results of hurricane Hugo).

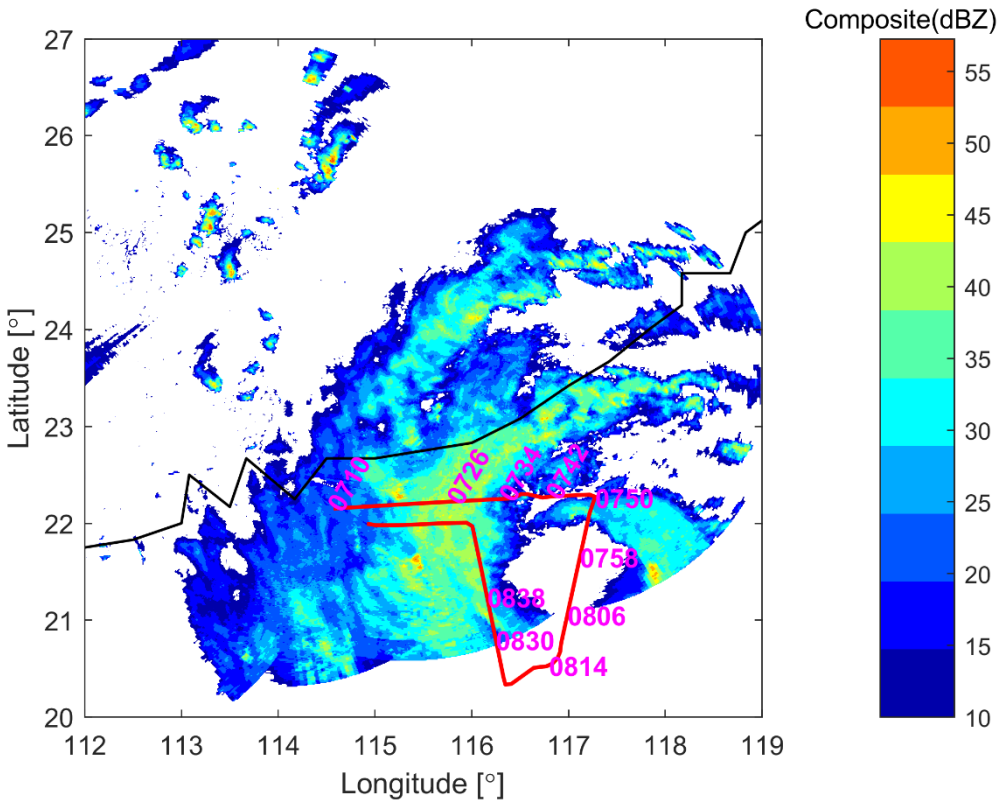

Fig 9 The projection of the flight path on the composite radar reflectivity at 3 km height at 0812 UTC 1 August 2016 from the South China weather radar network. The 4-digit number represents the UTC time of the flight. The black solid line is part of China mainland coastline.

Table 1. Summary of observation and calculation results for 9 flights through the 5 tropical cyclones. The variables included in the table are as follows: serial number(#), start time(UTC), end time(UTC), observation height z(m), average wind speed U_{zm} (m s^{-1}), momentum flux τ (kg m^{-1} s^{-2}), turbulence kinetic energy e (m^2s^{-2}), vertical wind speed standard deviation σ_w (m s^{-1}),True air speed Tas (m s^{-1}), kinetic energy dissipation rate ε (m^2 s^{-3}), vertical diffusion coefficients K_1, K_2 (m^2 s^{-1}), vertical mixing length ι (m), stationarity test index *IST* and corresponding tropical cyclone name, number and intensity.

#	Tst	Tnd	z	U_{zm}	τ	e	σ_w	Tas	ε	K_1	K_2	ι	*IST*	Tropical Cyclone
1	08/01/2013 0147	0155	499.5	13.9	0.05	0.35	0.48	111.5	2.74E-04	43.9	31.8	258.4	0.07	Jebi
2	08/01/2013 0155	0203	502.6	14.4	0.06	0.42	0.42	112.9	3.29E-04	29.8	36.9	184.7	0.05	1309, TS
3	08/01/2013 0203	0211	512.5	16.5	0.11	0.78	0.57	106.2	5.19E-04	59.0	82.9	275.3	0.05	
4	08/01/2013 0211	0219	519.7	17.3	0.11	0.68	0.48	104.3	5.69E-04	37.9	57.7	193.0	0.03	
5	08/01/2013 0219	0227	525.8	18.3	0.15	0.71	0.54	102.7	6.45E-04	45.6	54.8	215.0	0.07	
6	09/15/2014 0004	0012	945.4	17.1	0.06	0.31	0.39	112.7	4.44E-04	16.4	14.9	109.5	0.06	Kalmaegi
7	09/15/2014 0017	0025	611.8	20.0	0.24	1.02	0.65	110.3	1.63E-03	42.4	44.4	161.3	0.01	1415, Typhoon
8	09/15/2014 0025	0033	607.4	22.0	0.21	0.66	0.57	110.1	1.24E-03	47.4	24.6	187.7	0.03	
9	09/15/2014 0033	0041	599.2	24.8	0.38	1.41	0.80	108.0	4.88E-03	32.8	28.7	101.2	0.04	
10	09/15/2014 0041	0049	594.4	26.0	0.84	2.82	1.17	105.0	9.57E-03	58.9	58.1	132.6	0.08	
11	09/15/2014 0049	0057	582.5	28.9	0.48	3.48	1.27	105.5	9.04E-03	94.1	93.6	191.1	0.03	

12	09/15/2014 0057	0105	578.1	31.2	0.50	2.26	1.15	103.4	3.71E-03	108.1	96.4	265.1	0.03	
13	09/15/2014 0105	0113	567.3	31.7	0.29	2.81	1.07	104.3	8.77E-03	61.4	62.9	140.0	0.01	
14	09/15/2014 0113	0121	561.1	29.8	0.22	2.10	1.09	104.8	1.31E-02	27.6	23.4	69.3	0.13	
15	09/15/2014 0129	0137	554.6	29.1	0.13	2.09	1.21	102.7	7.13E-03	87.6	43.1	192.3	0.04	
16	09/15/2014 0137	0145	566.2	29.2	0.21	2.28	1.10	105.1	6.22E-03	59.0	58.7	148.0	0.05	
17	09/15/2014 0145	0153	582.2	31.3	0.48	3.72	1.35	106.8	3.30E-02	42.2	29.4	75.8	0.02	
18	09/15/2014 0153	0201	592.2	29.9	0.16	1.72	0.93	108.2	1.49E-02	24.8	13.9	62.1	0.01	
19	09/15/2014 0201	0209	600.1	26.8	0.07	1.37	0.88	111.3	1.26E-02	18.3	10.4	51.7	0.01	
20	09/15/2014 0209	0217	609.7	23.4	0.02	1.03	0.67	111.8	7.12E-03	11.8	10.5	42.8	0.01	
21	09/16/2014 0004	0012	594.5	26.9	0.05	1.74	0.50	115.9	8.96E-04	17.3	235.9	95.7	0.05	
22	09/16/2014 0012	0020	648.8	41.9	0.11	3.74	1.20	111.1	9.23E-03	41.3	106.1	102.6	0.05	
23	09/16/2014 0020	0028	635.1	42.7	0.33	3.28	1.26	109.3	2.58E-02	32.7	29.1	66.6	0.04	
24	09/16/2014 0028	0036	641.3	53.6	0.40	7.89	1.92	109.1	1.10E-01	46.1	39.6	60.0	0.03	
25	09/16/2014 0036	0044	673.8	62.2	1.32	7.07	2.02	113.5	7.03E-02	48.6	49.8	69.8	0.02	
26	07/08/2015 2324	2332	612.8	11.3	0.00	0.10	0.23	103.2	5.44E-05	10.1	12.2	129.2	0.06	Linfa
27	07/08/2015 2332	2340	603.8	18.6	0.03	0.50	0.42	103.2	1.55E-03	6.3	11.3	39.1	0.03	1510, severe TS

28	07/08/2015 2340	2348	604.6	26.8	0.33	2.60	0.96	102.0	1.69E-02	19.8	28.0	50.8	0.07	
29	07/08/2015 2348	2356	606.6	43.5	1.47	7.92	1.79	108.3	5.58E-02	65.0	78.7	91.9	0.05	
30	07/08/2015 2356	0004	617.3	55.6	0.95	4.08	1.33	110.3	1.60E-02	64.4	72.7	124.7	0.08	
31	07/09/2015 0004	0012	644.7	50.8	0.50	2.62	1.24	108.8	8.28E-03	163.0	58.1	295.1	0.07	
32	07/09/2015 0012	0020	621.6	53.8	1.42	7.43	1.82	110.8	5.41E-02	66.5	71.4	94.3	0.03	
33	07/09/2015 0020	0028	635.6	52.3	1.09	7.82	1.87	110.7	5.70E-02	64.6	75.1	91.0	0.05	
34	07/09/2015 0028	0036	645.2	36.8	0.63	2.43	1.11	107.1	1.48E-02	29.7	28.0	71.2	0.06	
35	07/09/2015 0036	0044	645.7	28.0	0.26	1.41	0.91	107.3	5.02E-03	33.3	27.6	101.7	0.05	
36	07/09/2015 0044	0052	611.4	30.5	0.13	0.86	0.59	107.8	4.18E-03	10.9	12.4	46.0	0.05	
37	07/09/2015 0052	0100	613.7	33.9	0.16	1.66	0.75	107.0	1.40E-02	10.1	13.9	32.1	0.05	
38	07/09/2015 0100	0108	617.3	33.2	0.67	3.84	1.43	105.7	3.95E-02	21.0	26.1	42.9	0.12	
39	10/03/2015 1018	1026	609.0	25.4	0.49	2.04	0.96	102.6	7.69E-03	43.6	39.4	111.9	0.10	Mujigae
40	10/03/2015 1026	1034	598.5	27.2	0.46	2.02	0.98	103.5	6.44E-03	54.8	46.2	138.8	0.01	1522, Typhoon
41	10/03/2015 1034	1042	604.5	29.4	0.68	2.66	1.10	102.3	6.98E-03	126.7	89.9	255.0	0.03	
42	10/03/2015 1042	1050	595.3	32.1	0.72	3.61	1.31	101.3	1.30E-02	76.9	70.9	150.3	0.02	
43	10/03/2015 1050	1058	608.5	32.2	0.50	2.45	1.03	100.3	6.60E-03	66.3	63.7	159.2	0.02	

44	10/03/2015 1058	1106	622.8	24.8	0.33	1.41	0.86	101.9	3.07E-03	58.3	44.6	174.9	0.01	
45	10/03/2015 1106	1114	618.8	21.9	0.06	1.26	0.79	103.5	1.23E-03	59.4	92.7	223.1	0.04	
46	10/03/2015 1114	1122	610.4	24.1	0.12	0.84	0.68	101.7	1.02E-03	99.9	57.8	345.2	0.04	
47	10/03/2015 1122	1130	578.1	26.0	0.13	1.12	0.81	102.6	3.37E-03	38.7	28.0	125.7	0.06	
48	10/03/2015 1138	1146	598.7	37.6	0.39	2.84	1.06	104.4	1.27E-02	33.6	40.8	81.2	0.02	
49	10/03/2015 1146	1154	599.7	41.4	0.71	3.06	1.14	103.4	1.65E-02	41.1	40.8	88.4	0.02	
50	10/03/2015 1154	1202	591.9	36.3	1.07	3.95	1.21	101.7	1.34E-02	123.2	90.9	212.2	0.04	
51	08/01/2016 0710	0718	651.7	11.3	0.07	0.28	0.31	135.4	5.02E-04	7.4	10.9	58.2	0.04	Nida
52	08/01/2016 0726	0734	616.0	32.3	0.11	1.17	0.80	135.1	5.00E-03	16.2	19.0	59.3	0.14	1604, strong Typhoon
53	08/01/2016 0734	0742	605.5	33.9	1.33	7.59	1.66	135.0	5.85E-02	50.8	69.0	75.5	0.02	
54	08/01/2016 0742	0750	611.7	35.1	1.06	4.99	1.25	135.5	2.27E-02	39.1	76.7	78.5	0.01	
55	08/01/2016 0750	0758	578.8	36.4	0.62	3.71	1.31	136.5	2.42E-02	34.9	39.9	71.1	0.03	
56	08/01/2016 0758	0806	633.0	6.7	0.40	1.02	0.61	137.2	6.79E-04	52.7	107.0	236.6	0.14	
57	08/01/2016 0806	0814	648.7	31.2	0.26	4.48	1.53	136.0	8.28E-02	13.1	17.0	25.0	0.11	
58	08/01/2016 0814	0822	635.5	33.4	0.13	3.38	0.96	135.3	9.70E-02	3.1	8.3	8.2	0.01	
59	08/01/2016 0830	0838	557.3	35.4	0.19	4.15	1.20	135.4	3.04E-02	20.0	39.8	44.2	0.08	

60	08/01/2016 0838	0846	612.0	38.8	1.46	10.53	2.00	135.2	1.07E-01	57.6	72.5	71.3	0.02	

Using the two methods described in the data processing section, we estimated the vertical eddy diffusivity K, with specific values shown in Table 1, and the relationship between the vertical eddy diffusivity and wind speed is shown in Fig.10. It can be seen that most of the K values estimated by the two methods fall below 100 m^2 s^{-1} (total 5 samples were above 100 m^2 s^{-1}, four of which were obtained during strong Typhoon Nida). As the analysis in the spectrum subsection, the eddies with a horizontal scale >10 km dominated the sign of covariance or flux. These legs are similar to the one seen in Hurricane Hugo where Extreme Vorticity Maximum (EVM) was observed. Zhang et al. (2011) cautioned that the flux data should not be used for comparing with standard flux parameterization in numerical models assuming stationarity.

For K from the *TKE* closing method, the wind speed ranged between 10 m s^{-1} and 40 m s^{-1}, the bin average value of K increases with wind speed from 15 to 62 m^2 s^{-1}. When the wind speed was above 40 m s^{-1}, K no longer increased with wind speed, showing a trend of saturation or weak attenuation. The trend of K obtained by the Hanna method with wind speed was similar to that obtained by the turbulence kinetic energy closing method, except that the interval of wind speed corresponding to K saturation was slightly lower, at about 30-35 m s^{-1}, and the bin average values of K varied from 16 to 90 m^2 s^{-1}. The results from the Hanna method were slightly larger than those obtained from the *e* closing method overall, and the ratio of the average values between the two intervals was 1.25 on average. Compared with the results of Zhang et al. (2011a), the K values obtained by the *e* closure and Hanna methods in this paper are very close under the same wind speed, although the observation heights of the two studies were different, which may be a major reason for the obvious difference in momentum fluxes.

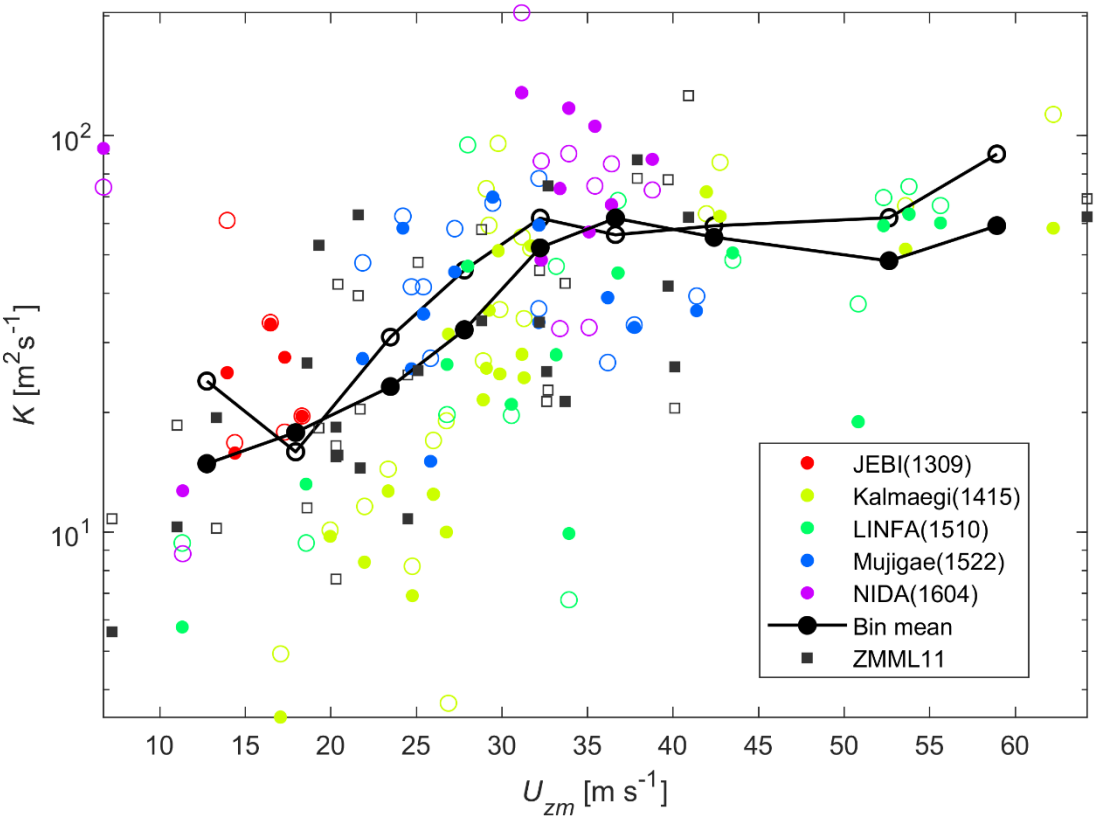

Fig.10 Log–linear plot of the vertical eddy diffusion coefficient as a function of the mean wind speed, with different colors representing different typhoon data, the solid markers representing *K* estimated via the *e* closing method, and the hollow markers representing *K* estimated by the Hanna method. The average values of *K* obtained via the two methods within each wind speed range of 5 m s^{-1} (a data point below 10 m s^{-1} is ignored in statistics and two data points above 55 m s^{-1} are classified as a bin) are indicated by a solid line with solid black dots and hollow black dots, respectively. We also include the results of Zhang et al. (2011a) in the figure.

Variation in vertical mixing length with wind speed is shown in Fig. 11 and the main body(55%) of vertical mixing length is within about 50-150 m, with an average value of 110 m, which is in good agreement with the typical vertical mixing length scale (Kepert 2012). There seems no explicit dependence of mixing length on wind speed given the scatter of the samples. The result of Zhang et al. (2011a) also show no dependence on wind speed.

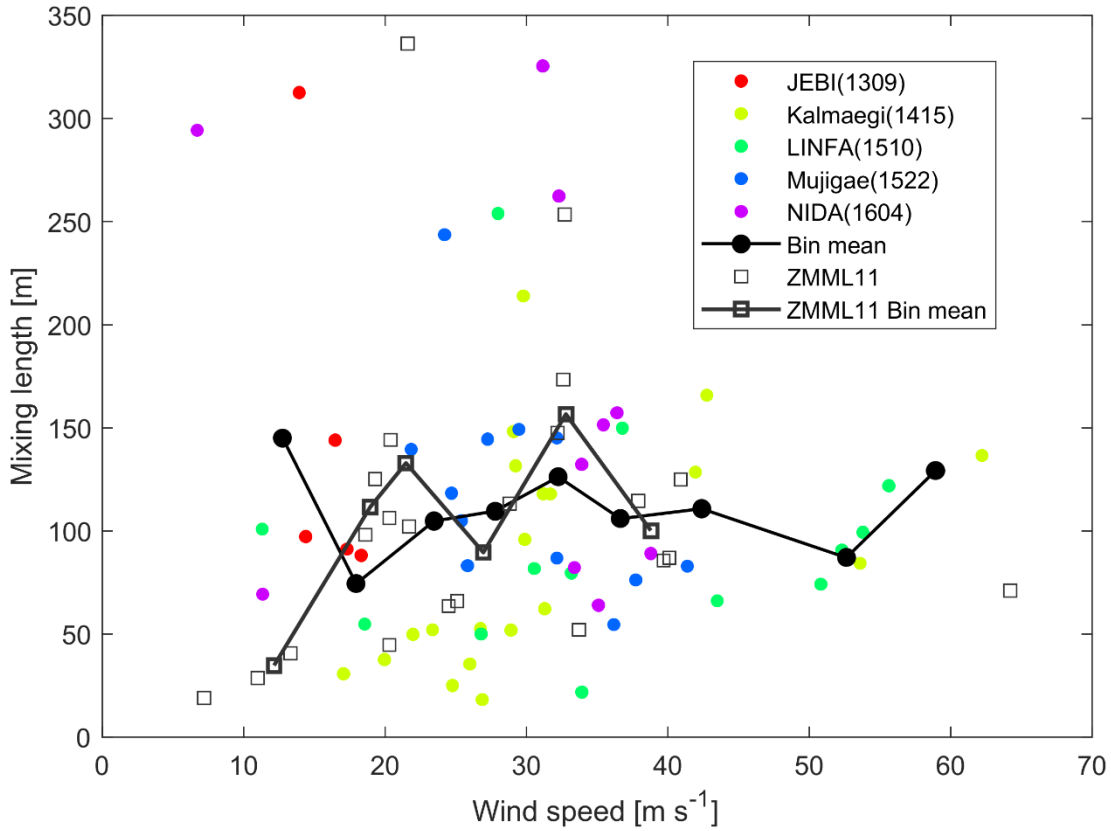

Fig. 11 Same as Fig. 7, but for the vertical mixing length

The profiles of τ, e, K, vertical mixing length and wind speed are shown in Fig. 12. It can be seen that τ and e profiles are very similar to that of U. So changes in τ and e quantity with height may be considered, to a large extent, a reflection of the corresponding change in wind speed with height. However, the dependence of K and mixing length on height is not significant and the bin averages of the two values remain approximately constant. Although there is only one observation value above 700 m at 945 m, τ, e, K and vertical mixing length are all close to 0, consistent with the behavior of these physical quantities near the top of the boundary layer as expected.

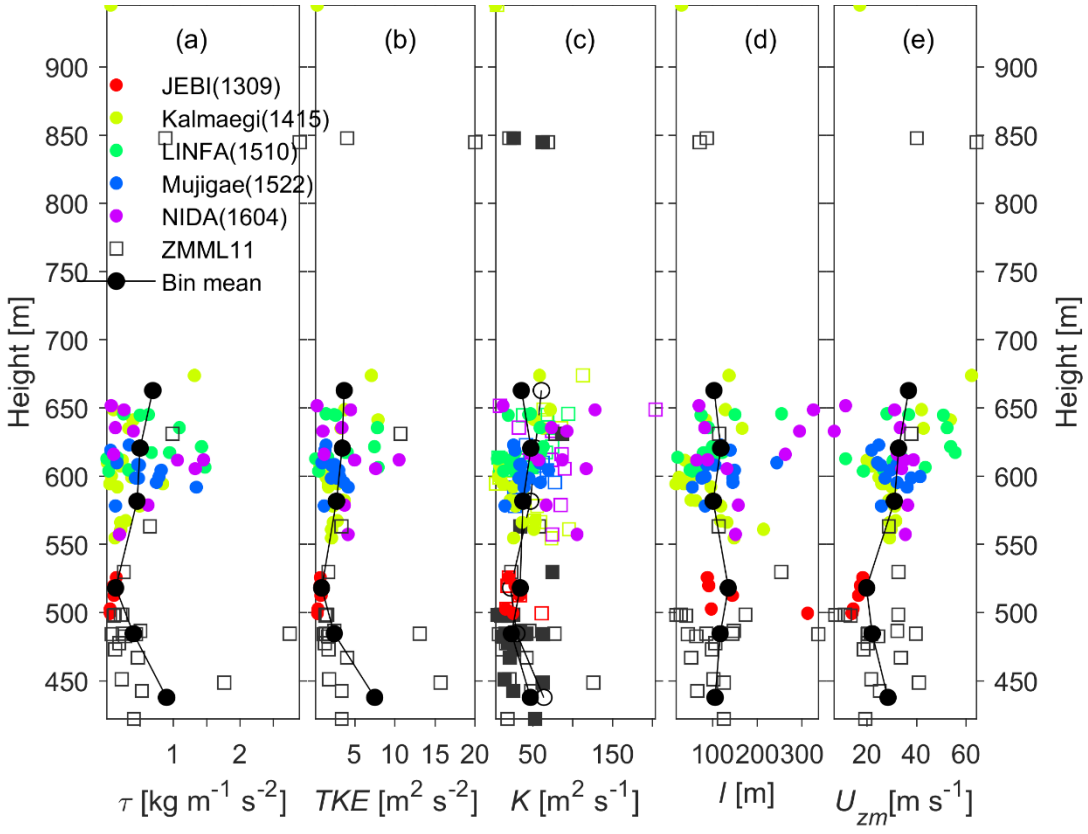

Fig. 12(a) Momentum flux, (b) turbulence kinetic energy *e*, (c) *K*, (d) mixing length l and (e) wind speed with height; all the subpanels share the same legends as in (a), with black dots representing bin mean values of each 50 m height bin from 400 to 700 m height and the hollow black dots in (c) correspond to the Hanna method.

In one of the commonly used first order nonlocal parameterization scheme of vertical eddy momentum diffusitivity(Kepert 2012), the *K*-profile parameterization scheme, the expression of *K* is

$$K = \kappa u_{*_s} z(1 - z/h)^p \tag{8}$$

where κ is the von Karman constant ($\kappa = 0.4$), u_{*_s} is the friction velocity in the surface layer, e.g, 10 m, h is the boundary layer height and p is the shape exponent. Here, we use the inflow layer height below which the radial wind is toward the center of a TC as the boundary layer height. A relationship between the inflow layer height and the distance to the TC center normalized by the radius of maximum wind (RMW) is obtained by fitting the curve in the top-right panel of Fig.10 in Zhang et al. (2011b). The RMW of each typhoon is estimated according to the aircraft measurements, the

radar reflectivity and the best track data. For the five TCs Jebi(1309), Kalmaegi(1415), Linfa(1510), Mujigae(1522) and Nida(1604), the RMWs are 75, 98, 35, 40, and 77 km, respectively. Then the distance of each sample to the TC center is normalized by the corresponding RMW. The boundary layer height for each sample is then estimated using the relationship and the normalized distance.

The surface layer friction velocity u_{*_S} is obtained by correcting the vertical gradient of friction velocity induced by horizontal pressure gradient following Donelan (1990).

$$u_*^2 = u_{*_S}^2 - Af_c z u_{*_S} \tag{9}$$

Where A is a constant about 12 in neutral condition(Donelan 1990), f_c is the Coriolis parameter, and u_* is the friction velocity at height z. More details are referred to (Donelan 1990).

The K-profile scheme is evaluated with our observations as shown in Fig. 13. The shape exponent is fitted to a value about 1.72 with a 95% confidence interval [1.33 2.12]. In ensemble prediction, the shape exponent was set to be perturbed stochastically in a range of [1 3] and found to be one of the first-ranked sensitive parameters for the simulation of convection and precipitation(Di et al. 2015). Here we provide the observations indicating that the shape exponent is not a constant.

The vertical mixing length scale is formulated by (Blackadar 1962) as

$$\frac{1}{l} = \frac{1}{\kappa z} + \frac{1}{l_\infty} \tag{10}$$

Where l_∞ is the asymptotic mixing length. This formula is fitted using the data here.

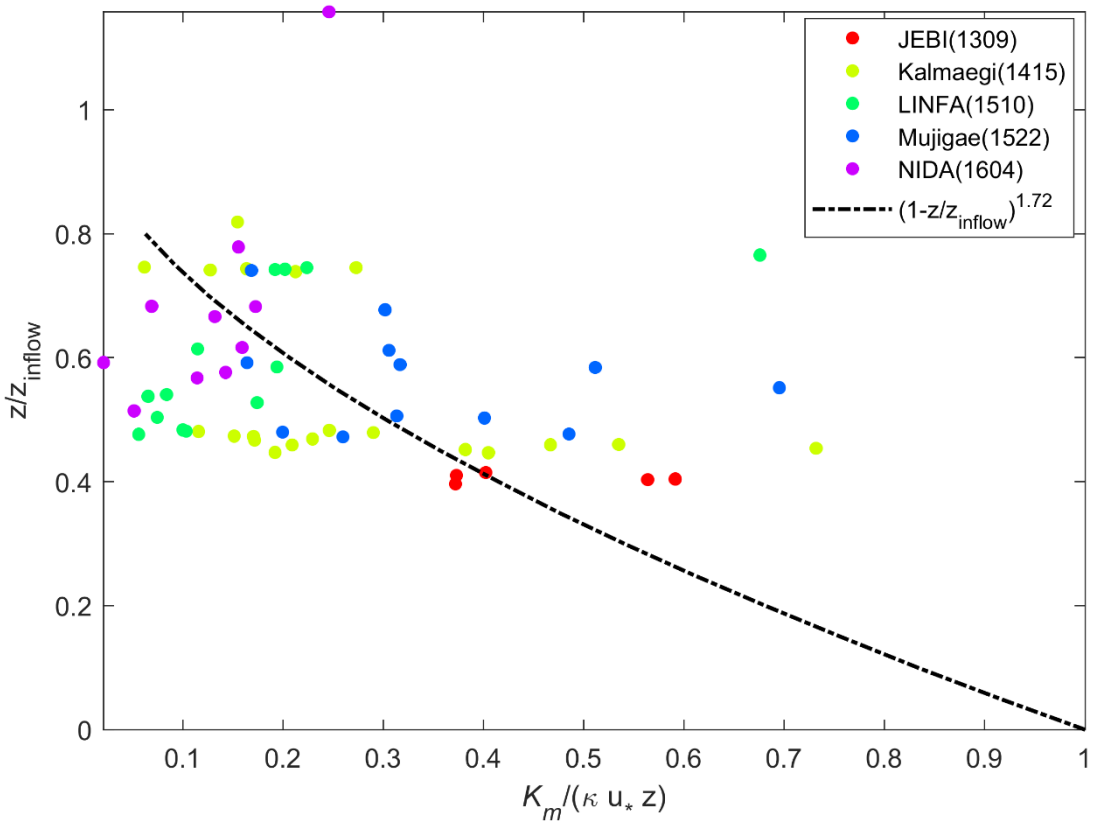

Fig. 13 Dependence of Eddy diffusivity scaled by $\kappa u_{*_s} z$ on the dimensionless height normalized by the inflow layer height.

4 Discussion and Conclusion

In this paper, we analyzed turbulence characteristics in the boundary layer of typhoons based on atmospheric boundary layer data (observation height concentrated around 500 to 700 m) collected during six reconnaissance flights through five TCs over the South China coast as operated by the Hong Kong Observatory. The co-spectra of horizontal wind speed components and vertical wind speed and their cumulative spectra (ogive) showed that the horizontal scale of turbulent vortices contributed significantly to flux in a range of 1 to 10 km, while the magnitude of the vertical mixing length was about 100 m. The ratio of the horizontal scale to the vertical mixing length of the turbulent eddy was estimated to be 10 to 100, so the observed turbulent eddy at the boundary layer of the typhoon can be regarded as having a two-dimensional structure.

Statistical analysis of τ and e showed that in the wind speed range of 10 to 36 m s^{-1}, these two physical quantities increased with wind speed, and then no longer increased significantly with wind speed in the range >36 to about 62 m s^{-1}.

We estimated the vertical eddy diffusion coefficient K by using the Hanna method (Hanna 1968) as well as the turbulence kinetic energy closing method. The results obtained using these two methods were essentially consistent. Within a certain wind speed range (< 40 m s^{-1}), K increases with wind speed monotonically, and then K does not increase further, or even decrease.

In conjunction with previous research results, we also analyzed the relationship between the above physical quantities and height, and learned that the changes of τ, e and K with height were mainly caused by a change in wind speed with height, while there seem no explicit dependence of vertical mixing length on height.

Acknowledgement: We are grateful to scientists and crew members who participated the field work that helped corrected the aircraft data used in this study. Zhongkuo Zhao was sponsored by the National Major Fundamental Research Program of China (Grant No. 2015CB452802), the National Natural Science Foundation (Grant No. 41875021, 41830533, 41675021). Jun Zhang was supported by Grant NA14NWS4680028, and NSF Grants AGS1822128 and ASG1654831.

Appendix

References

Beswick, K. M., M. W. Gallagher, A. R. Webb, E. G. Norton and F. Perry (2008) Application of the Aventech AIMMS20AQ airborne probe for turbulence measurements during the Convective Storm Initiation Project. Atmos Chem Phys 8(17): 5449-5463.

Black, P. G., E. A. D'Asaro, W. M. Drennan, J. R. French, P. P. Niiler, T. B. Sanford, E. J. Terrill, E. J. Walsh and J. A. Zhang (2007) Air–Sea Exchange in Hurricanes: Synthesis of Observations from the Coupled Boundary Layer Air–Sea Transfer Experiment. Bull Am Meteorol Soc 88(3): 357-374.

Blackadar, A. K. (1962) The vertical distribution of wind and turbulent exchange in a neutral atmosphere.

Journal of Geophysical Research (1896-1977) 67(8): 3095-3102.

Chan, P. W., W. K. Wong and K. K. Hon (2014) Weather observations by aircraft reconnaissance inside Severe Typhoon Utor. Weather 69(8): 199-202.

Charney, J. G. and A. Eliassen (1964) On the Growth of the Hurricane Depression. J Atmos Sci 21(1): 68-75.

Coronel, R., M. Sawada and T. Iwasaki (2016) Impacts of Surface Drag Coefficient and Planetary Boundary Layer Schemes on the Structure and Energetics of Typhoon Megi (2010) during Intensification. J Meteorol Soc Jpn Ser II 94(1): 55-73.

Di, Z., Q. Duan, W. Gong, C. Wang, Y. Gan, J. Quan, J. Li, C. Miao, A. Ye and C. Tong (2015) Assessing WRF model parameter sensitivity: A case study with 5 day summer precipitation forecasting in the Greater Beijing Area. Geophys Res Lett 42(2): 579-587.

Donelan, M. A. (1990). Air-sea interaction. The Sea. edited by B. LeMehaute and D. M. Hanes, John Wiley and Sons, 239-292.

Drennan, W. M., J. A. Zhang, J. R. French, C. McCormick and P. G. Black (2007) Turbulent Fluxes in the Hurricane Boundary Layer. Part II: Latent Heat Flux. J Atmos Sci 64(4): 1103-1115.

Etling, D. and R. A. Brown (1993) Roll vortices in the planetary boundary layer: A review. Boundary-Layer Meteorol 65(3): 215-248.

Fang, J., J. Tang and R. Wu (2009) The effect of surface friction on the development of tropical cyclones. Adv Atmos Sci 26(6): 1146.

Foken, T. and B. Wichura (1996) Tools for quality assessment of surface-based flux measurements. Agr Forest Meteorol 78(1): 83-105.

Foster, R. C. (2009) Boundary-Layer Similarity Under an Axisymmetric, Gradient Wind Vortex. Boundary-Layer Meteorol 131(3): 321-344.

Foster, S. and P. W. Chan (2012) Improving the wind and temperature measurements of an airborne meteorological measuring system. J Zhejiang Univ Sci A 13(10): 723-746.

French, J. R., W. M. Drennan, J. A. Zhang and P. G. Black (2007) Turbulent Fluxes in the Hurricane Boundary Layer. Part I: Momentum Flux. J Atmos Sci 64(4): 1089-1102.

Gall, R., J. Tuttle and P. Hildebrand (1998) Small-Scale Spiral Bands Observed in Hurricanes Andrew,

Hugo, and Erin. Mon Weather Rev 126(7): 1749-1766.

Gopalakrishnan, S. G., F. Marks, J. A. Zhang, X. Zhang, J.-W. Bao and V. Tallapragada (2013) A Study of the Impacts of Vertical Diffusion on the Structure and Intensity of the Tropical Cyclones Using the High-Resolution HWRF System. J Atmos Sci 70(2): 524-541.

Hanna, S. R. (1968) A Method of Estimating Vertical Eddy Transport in the Planetary Boundary Layer Using Characteristics of the Vertical Velocity Spectrum. J Atmos Sci 25(6): 1026-1033.

Holt, T. and S. Raman (1988) A review and comparative evaluation of multilevel boundary layer parameterizations for first-order and turbulent kinetic energy closure schemes. Rev Geophys 26(4): 761-780.

Kepert, J. D. (2012) Choosing a Boundary Layer Parameterization for Tropical Cyclone Modeling. Mon Weather Rev 140(5): 1427-1445.

Kilroy, G., M. T. Montgomery and R. K. Smith (2017) The role of boundary-layer friction on tropical cyclogenesis and subsequent intensification. Q J Roy Meteorol Soc 143(707): 2524-2536.

Li, Q., Y. Duan, H. Yu and G. Fu (2010) Finescale spiral rainbands modeled in a high-resolution simulation of Typhoon Rananim (2004). Adv Atmos Sci 27(3): 685-704.

Liu, J., F. Zhang and Z. Pu (2017) Numerical simulation of the rapid intensification of Hurricane Katrina (2005): Sensitivity to boundary layer parameterization schemes. Adv Atmos Sci 34(4): 482-496.

Ming, J. and J. A. Zhang (2018) Direct Measurements of Momentum Flux and Dissipative Heating in the Surface Layer of Tropical Cyclones During Landfalls. J Geophys Res Atmos 123(10): 4926-4938.

Morrison, I., S. Businger, F. Marks, P. Dodge and J. A. Businger (2005) An Observational Case for the Prevalence of Roll Vortices in the Hurricane Boundary Layer. J Atmos Sci 62(8): 2662-2673.

Nieuwstadt, F. T. M. (1984) The Turbulent Structure of the Stable, Nocturnal Boundary Layer. J Atmos Sci 41(14): 2202-2216.

Ooyama, K. (1969) Numerical Simulation of the Life Cycle of Tropical Cyclones. J Atmos Sci 26(1): 3-40.

Pendergrass, A. G. and H. E. Willoughby (2009) Diabatically Induced Secondary Flows in Tropical Cyclones. Part I: Quasi-Steady Forcing. Mon Weather Rev 137(3): 805-821.

Powell, M. D., P. J. Vickery and T. A. Reinhold (2003) Reduced drag coefficient for high wind speeds in

tropical cyclones. Nature 422: 279.

Rai, D. and S. Pattnaik (2018) Sensitivity of Tropical Cyclone Intensity and Structure to Planetary Boundary Layer Parameterization. Asia-Pacific J Atmos Sci 54(3): 473-488.

Shapiro, L. J. and H. E. Willoughby (1982) The Response of Balanced Hurricanes to Local Sources of Heat and Momentum. J Atmos Sci 39(2): 378-394.

Tang, J., J. A. Zhang, S. D. Aberson, F. D. Marks and X. Lei (2018) Multilevel Tower Observations of Vertical Eddy Diffusivity and Mixing Length in the Tropical Cyclone Boundary Layer during Landfalls. J Atmos Sci 75(9): 3159-3168.

Tennekes, H. (1973) The Logarithmic Wind Profile. J Atmos Sci 30(2): 234-238.

Trauth, M. H. (2015). Time-Series Analysis. MATLAB® Recipes for Earth Sciences. edited by. Berlin, Heidelberg, Springer Berlin Heidelberg, 151-213.

Wang, Y. (2001) An Explicit Simulation of Tropical Cyclones with a Triply Nested Movable Mesh Primitive Equation Model: TCM3. Part I: Model Description and Control Experiment. Mon Weather Rev 129(6): 1370-1394.

Wong, M. L. M. and J. C. L. Chan (2006) Tropical Cyclone Motion in Response to Land Surface Friction. J Atmos Sci 63(4): 1324-1337.

Xia, H., M. Shats and G. Falkovich (2009) Spectrally condensed turbulence in thin layers. Phys Fluids 21(12): 125101.

Zhang, F. and Z. Pu (2017) Effects of Vertical Eddy Diffusivity Parameterization on the Evolution of Landfalling Hurricanes. J Atmos Sci 74(6): 1879-1905.

Zhang, F., Z. Pu and C. Wang (2017a) Effects of Boundary Layer Vertical Mixing on the Evolution of Hurricanes over Land. Mon Weather Rev 145(6): 2343-2361.

Zhang, J. A., P. G. Black, J. R. French and W. M. Drennan (2008) First direct measurements of enthalpy flux in the hurricane boundary layer: The CBLAST results. Geophys Res Lett 35(14).

Zhang, J. A. and W. M. Drennan (2012) An Observational Study of Vertical Eddy Diffusivity in the Hurricane Boundary Layer. J Atmos Sci 69(11): 3223-3236.

Zhang, J. A., W. M. Drennan, P. G. Black and J. R. French (2009) Turbulence Structure of the Hurricane Boundary Layer between the Outer Rainbands. J Atmos Sci 66(8): 2455-2467.

Zhang, J. A., F. D. Marks, M. T. Montgomery and S. Lorsolo (2011a) An Estimation of Turbulent Characteristics in the Low-Level Region of Intense Hurricanes Allen (1980) and Hugo (1989). Mon Weather Rev 139(5): 1447-1462.

Zhang, J. A., F. D. Marks, J. A. Sippel, R. F. Rogers, X. Zhang, S. G. Gopalakrishnan, Z. Zhang and V. Tallapragada (2018) Evaluating the impact of improvement in the horizontal diffusion parameterization on hurricane prediction in the operational Hurricane Weather Research and Forecast (HWRF) Model. Weather Forecast 33(1): 317-329.

Zhang, J. A., R. F. Rogers, D. S. Nolan and F. D. M. Jr. (2011b) On the Characteristic Height Scales of the Hurricane Boundary Layer. Mon Weather Rev 139(8): 2523-2535.

Zhang, J. A., R. F. Rogers and V. Tallapragada (2017b) Impact of Parameterized Boundary Layer Structure on Tropical Cyclone Rapid Intensification Forecasts in HWRF. Mon Weather Rev 145(4): 1413-1426.

Zhao, Z.-K., C.-X. Liu, Q. Li, G.-F. Dai, Q.-T. Song and W.-H. Lv (2015) Typhoon air-sea drag coefficient in coastal regions. J Geophys Res: Oceans 120(2): 716-727.

Zhu, P. and J. Furst (2013) On the parameterization of surface momentum transport via drag coefficient in low-wind conditions. Geophys Res Lett 40(11): 2824-2828.

Zhu, P., K. Menelaou and Z. Zhu (2014) Impact of subgrid-scale vertical turbulent mixing on eyewall asymmetric structures and mesovortices of hurricanes. Q J Roy Meteorol Soc 140(679): 416-438.

Zhu, P., Y. Wang, S. S. Chen, M. Curcic and C. Gao (2015) Impact of storm-induced cooling of sea surface temperature on large turbulent eddies and vertical turbulent transport in the atmospheric boundary layer of Hurricane Isaac. J Geophys Res: Oceans 121(1): 861-876.

Zhu, P., J. A. Zhang and F. J. Masters (2010) Wavelet Analyses of Turbulence in the Hurricane Surface Layer during Landfalls. J Atmos Sci 67(12): 3793-3805.